



Interface states modulation in Pt/Graphene/GaN Schottky barrier diodes

Junxue Ran ^{a,b,c}, Yijian Song ^{a,b,c}, Xiaoli Ji ^{a,b,c}, Renfeng Chen ^{a,b,c}, Jiankun Yang ^{a,b,c}, Junxi Wang ^{a,b,c}, Tongbo Wei ^{a,b,c,*}

^a State Key Laboratory of Solid-State Lighting, Institute of Semiconductors, Chinese Academy of Sciences, Beijing, China

^b Center of Materials Science and Optoelectronics Engineering, University of Chinese Academy of Sciences, Beijing, 100049, China

^c The Beijing Engineering Research Center for the 3rd Generation Semiconductor Materials and Application, Beijing, 100083, China



ARTICLE INFO

Keywords:
GaN
Graphene
Schottky barrier diodes
Capacitance-conductance characteristics
Interface states

ABSTRACT

Recently Graphene (Gr) becomes a promising candidate for the integration of devices as a Schottky contact. In this study, Pt/Gr/GaN and Pt/GaN SBDs were fabricated to determine the Gr interlayer effect on the electrical characteristics of the devices. The temperature and frequency dependent capacitance-voltage ($C-V$), conductance-voltage ($G/\omega-V$), and current-voltage ($I-V$) are measured, from which the Schottky barrier height (SBH), reverse leakage, the density of interface states (N_{ss}), and time constants are derived. The results reveal SBDs with Gr interlayer exhibited higher SBH and lower leakage current. The N_{ss} for the Pt/GaN SBD were in the range of 2×10^{13} to $2.33 \times 10^{13} \text{ eV}^{-1}\text{cm}^{-2}$ at ($E_C - 0.35$) to ($E_C - 0.62$) eV, while the value for Pt/Gr/GaN SBD varies in the range of 1.85×10^{13} to $2.02 \times 10^{13} \text{ eV}^{-1}\text{cm}^{-2}$ at ($E_C - 0.57$) to ($E_C - 0.84$) eV. The N_{ss} of Pt/Gr/GaN is reduced and the distribution shifts toward the mid-gap of GaN in comparison with Pt/GaN. It is considered that the modulation of the interface states is attributed to the passivation of chemically inert Gr interlayer.

1. Introduction

High quality Schottky contact is particularly important in applications of Schottky-type devices such as Schottky barrier diodes (SBDs), high electron mobility transistors (HEMTs), and photodetector diodes (PDs). A variety of interlayers were incorporated in the Schottky contact stack to suppress the interface states and enhance the interface quality. Conventionally SiO₂ [1], Al₂O₃ [2,3], SiN_x [4,5], AlN [6], and some polymers [7–9], etc. have been employed as interlayer materials. Recently, two-dimensional graphene (Gr) has attracted a lot of attention as a potential Schottky contact. This stems from graphene's potential advantages such as high intrinsic electron mobility, quantum electronic transport [10], low optical absorption [11], mechanically strong and chemically stable for the C–C bonding with honeycomb structure, which is diffusion barrier against easy passage and prevents substitutional atomic migration from metallic alloys [12]. Gr used as Schottky contact, has been studied in a variety of semiconductors such as SiC, Si, and GaAs [13–16]. Some studies on Schottky contact between Gr and GaN or low aluminum AlGaN were also reported [17–23]. In most of the studies, the Gr was mainly employed as a contact material like metal however few works were reported on the use of Gr as an interlayer between metal and GaN [24,25]. In our previous work [26], the Pt/Gr/GaN sandwich

structure SBDs showed that Gr interlayer can significantly improve the performance of the GaN-based SBDs. However, the characteristics of interface states in Pt/Gr/GaN and the mechanism of effects on the performance of Schottky contact are not deeply understood yet.

In this work, the frequency and temperature-dependent $C-V$, $G/\omega-V$ and $I-V$ measurements are carried out in the wide frequency range of 1 kHz–1 MHz and the temperature range of 298–418 K. The basic electrical parameters in Pt-GaN SBDs with and without Gr interlayer were extracted respectively. The influence of the Gr interlayer on SBH, reverse leakage, N_{ss} and time constants are investigated comparatively. The possible effect mechanisms of Gr interlayer are presented. This work will provide more insight into the effects of the Gr interlayer on the interface states of the Pt/Gr/GaN SBDs.

2. Experimental details

The GaN epitaxial layers were grown by metal organic chemical vapor deposition (MOCVD) on the c-plane sapphire substrate. As shown in Fig. 1(a), the structure consists of a 2 μm undoped GaN layer, a 1 μm Si heavily doped n⁺-GaN (~3 × 10¹⁸ cm⁻³) layer, and a 3.5 μm Si doped n⁻-GaN (~3 × 10¹⁷ cm⁻³) layer. The quasi-vertical devices were fabricated with Ti/Al/Ti/Au (200/1000/200/1500 Å) for cathode ohmic

* Corresponding author. State Key Laboratory of Solid-State Lighting, Institute of Semiconductors, Chinese Academy of Sciences, Beijing, China.

E-mail address: tbwei@semi.ac.cn (T. Wei).

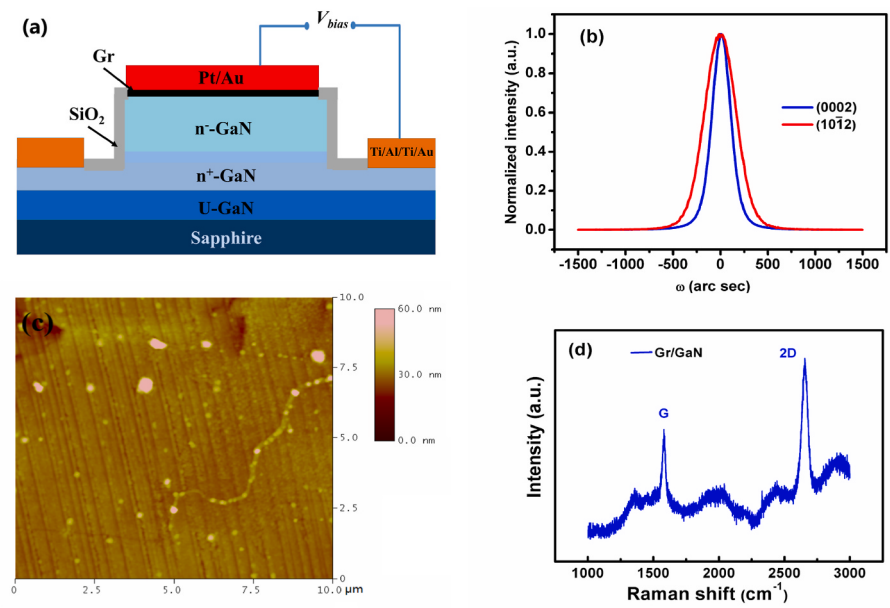


Fig. 1. (a) Schematic diagram of Pt/Gr/GaN SBD. (b) (0002) and (10 $\bar{1}$ 2) rocking curve of GaN by HRXRD. (c) AFM morphology and (d) Raman spectroscopy of Gr on GaN.

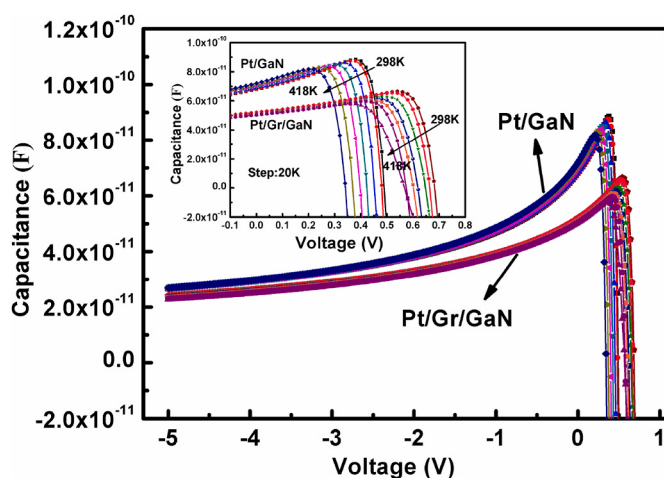


Fig. 2. Temperature-dependent C – V characteristics of Pt/GaN and Pt/Gr/GaN SBDs in the temperature range of 298–418 K at the frequency of 1 MHz. The inset shows the magnification of the C – V plots in forward bias.

contact on the n⁺-GaN etching surface and Pt/Au (300/2000 Å) on Gr/GaN for Schottky contact. The detailed devices and Gr transfer procedure can be found in the previous works [26,27]. The structural and surface qualities of the Gr/GaN were characterized. As shown in Fig. 1(b), the full width at half maximum (FWHM) of (0002) and (10 $\bar{1}$ 2) were 231arcsec and 382arcsec respectively using high-resolution x-ray diffraction (HRXRD), which indicate the good crystallinity. As shown in Fig. 1(c), The atomic force microscopy (AFM) morphology of Gr/GaN showed the peculiar corrugations in the Gr membrane. The Raman spectrum of Gr on GaN shown in Fig. 1(d), the primary in-plane vibrational mode of G peak (at 1582 cm⁻¹) and the double resonant 2D peak (at 2683 cm⁻¹) can be seen. The intensity of the D peak (at 1350 cm⁻¹) is negligible, indicating the high crystalline quality of transferred Gr. The comparative Pt/GaN SBDs were fabricated with the same procedures except Gr interlayer. The temperature and frequency dependence C – V and G/ω – V and I – V measurements were performed by a KEYSIGHT B1500 A semiconductor analyzer.

3. Results and discussion

The temperature-dependent C – V characteristics of Pt/GaN and Pt/Gr/GaN SBDs are measured in the range of 298–418 K with a step of 20 K. The measurement frequency is 1 MHz. As shown in Fig. 2. In the reverse bias region from –5 V to 0 V, the capacitance increases with the

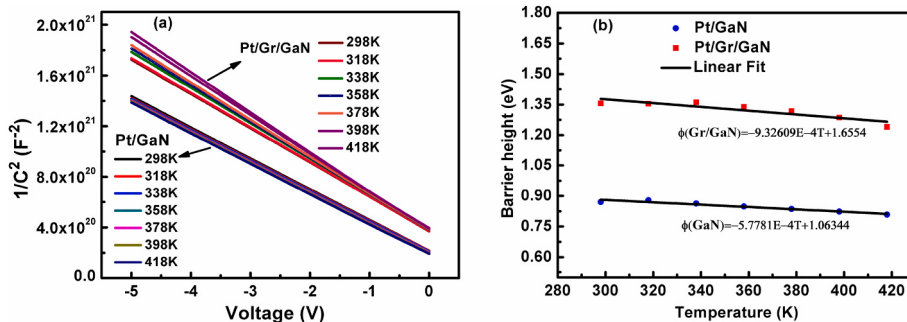


Fig. 3. (a) Temperature dependence $1/C^2$ – V plots of Pt/GaN and Pt/Gr/GaN in reverse bias. (b) the barrier height as a function of temperature determined from C – V measurements.

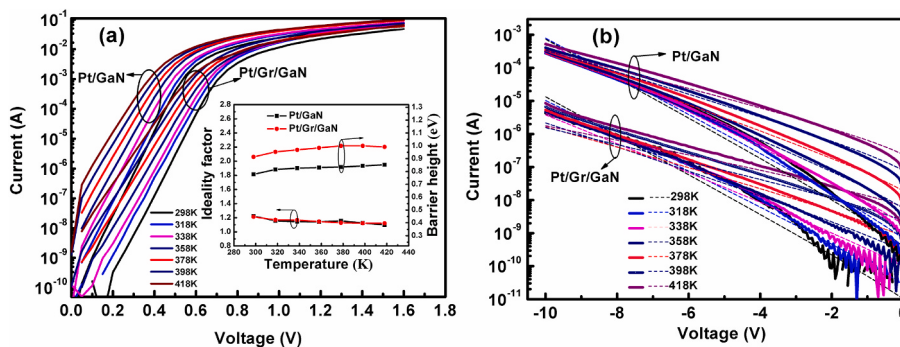


Fig. 4. The temperature-dependent plots of (a) forward I - V and (b) reverse I - V characteristics for Pt/GaN SBDs and Pt/Gr/GaN SBDs. The inset of (a) shows Schottky barrier height and ideality factor as a function of temperature. The solid lines are the measured data and the dotted lines are the fitting curves using the TFE model in (b).

decreasing reverse bias for all temperatures, while varies little with temperature for the same bias. In the forward bias, which is enlarged shown in the inset of Fig. 2, the capacitance increased to anomalous peak. The peak slightly decreases and shift toward the lower bias with the increasing temperature which is caused by the escape of the charges at the interface due to the temperature effect [28]. Comparing the forward bias C - V - T characteristics of Pt/Gr/GaN with Pt/GaN SBDs, it can be seen that the anomalous peaks for Pt/Gr/GaN is lower and shift to a relatively higher applied bias than that of Pt/GaN. This could be related to the effects of Gr interlayer on the Schottky contact with respect to SBH, N_{ss} which are further investigated.

The reverse bias $1/C^2$ - V - T plots are shown in Fig. 3(a). The built-in voltage V_{bi} and net donor concentration N_D can be extracted by using the formula [29]:

$$\frac{1}{C^2} = \frac{2}{q\epsilon_s\epsilon_0 N_D} (V_{bi} - V - kT/q) \quad (1)$$

where k is the Boltzmann constant, q is the electron charge, and T is the absolute temperature, ϵ_0 is the vacuum permittivity and ϵ_s is the relative permittivity of GaN. The $1/C^2$ - V plots of both Pt/GaN and Pt/Gr/GaN devices show very good linearity, which indicates that the net

donor concentration is nearly uniform along the depth direction. The Schottky barrier height $\phi_{B,CV}$ is given by:

$$q\phi_{B,CV} = qV_{bi} - q\phi_{IL} + (E_C - E_F) \quad (2)$$

where ϕ_{IL} , E_C , E_F are the image-force-induced barrier height lowering, bottom of the conduction band and the Fermi level position, respectively. Fig. 3(b) plots the extracted Schottky barrier height $\phi_{B,CV}$ as a function of operating temperature. As shown in Fig. 3(b), the $\phi_{B,CV}$ of Pt/Gr/GaN SBDs is higher than that of Pt/GaN SBDs. The introduction of Gr interlayer between Pt and GaN leads to an increase in $\phi_{B,CV}$ from 0.89 eV to 1.35 eV at room temperature. The values of $\phi_{B,CV}$ slightly decrease with increasing temperature for both devices. This may be originated from the bandgap shrinkage in GaN with increasing temperature [30]. The temperature dependence of the $\phi_{B,CV}$ can be approximated as

$$\phi_{B,CV} = \phi_{B0}(T=0K) + \alpha T \quad (3)$$

here ϕ_{B0} is the barrier height at absolute zero temperature, and α is the temperature coefficient of the barrier height. The α can be obtained from the linear fit of (3) to the data shown in Fig. 3(b). The values of α are -5.8×10^{-4} eV/K and -9.3×10^{-4} eV/K for Pt/GaN and Pt/Gr/GaN,

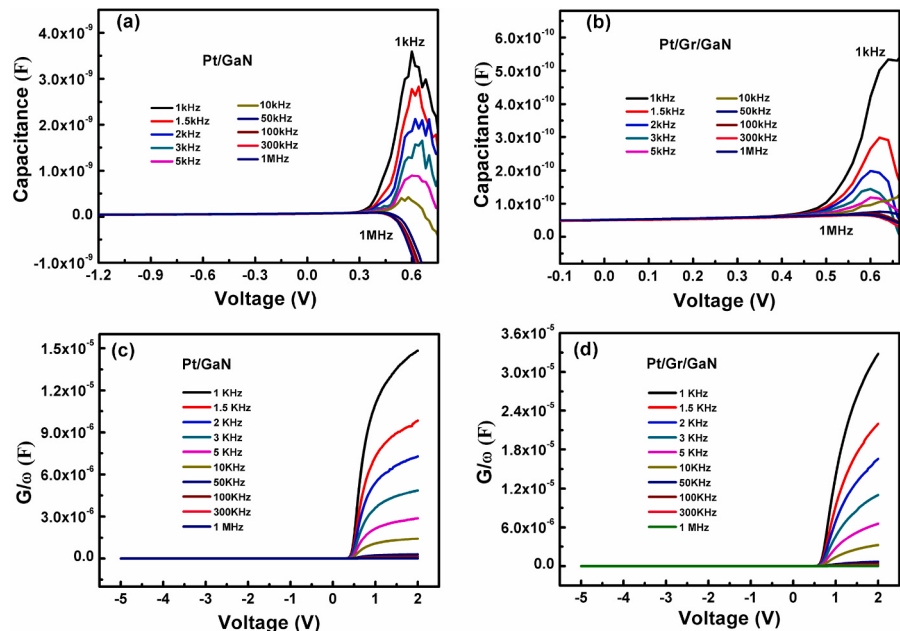


Fig. 5. The measured C - V characteristics of (a) Pt/GaN and (b) Pt/Gr/GaN SBDs, and G/ω - V characteristics of (c) Pt/GaN and (d) Pt/Gr/GaN SBDs in the frequency range of 1 kHz-1MHz at room temperature.

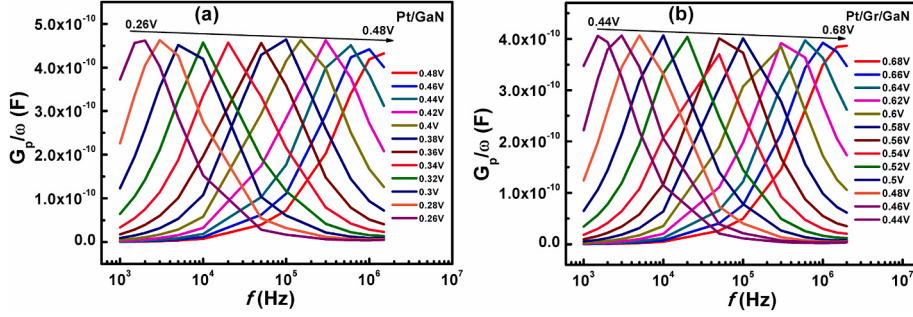


Fig. 6. G_p/ω - f characteristics at various biases derived from measured conductance data for the sample of (a) Pt/GaN (b) Pt/Gr/GaN.

respectively, which are comparable to that have been reported in previous works [30,31].

Temperature-dependent forward and reverse I - V characteristics of Pt/GaN and Pt/Gr/GaN SBDs are shown in Fig. 4(a)-(b) respectively. According to the thermionic emission model, the forward current can be expressed as [29,32]:

$$I = I_0 \left[\exp \left(\frac{qV}{nKT} \right) - 1 \right] \quad (4)$$

$$I_0 = AA^*T^2 \exp \left(-\varphi_{B,IV}/kT \right) \quad (5)$$

where I_0 is the saturation current, $\varphi_{B,IV}$ is the barrier height, A is the contact area, A^* is the Richardson constant ($26.4 \text{ A cm}^{-2} \text{ K}^{-2}$ for GaN). The $\varphi_{B,IV}$ and ideality factor n at different temperatures are determined and plotted in the inset of Fig. 4(a). The $\varphi_{B,IV}$ with Gr interlayer is higher than that without Gr interlayer. This is consistent with the C - V results which imply the Schottky barrier is enhanced for the Gr interlayer. As shown in Fig. 4(b), the diodes with Gr interlayer exhibit lower leakage current than that without Gr interlayer. Due to the higher SBH, leakage current through thermionic emission would be negligibly small and cannot be the primary leakage. Here the theoretical calculation is carried out based on the thermionic field emission (TFE) model. The TFE reverse current (I_{TFE}) can be described by the following equation [33]:

$$I_{TFE} = \frac{A^*ATq\hbar E}{k} \sqrt{\frac{\pi}{2m_n kT}} \times \exp \left[-\frac{1}{kT} \left(\varphi_{B,IV} - \frac{(q\hbar E)^2}{24m_n(kT)^2} \right) \right] \quad (6)$$

where \hbar is the reduced Planck constant, m_n is the electron effective mass, E is the electric field at the Schottky contact interface expressed as $E = \sqrt{2qN_D(V_{bi} - V)/(e_0\epsilon_r)}$. The built-in voltage V_{bi} and net donor concentration N_D are extracted from the C - V measurements. As shown by the dotted lines in Fig. 4(b), both devices with and without Gr can be well fitted by the TFE model. The improved leakage characteristics of Pt/Gr/GaN are attribute to the Gr interlayer which increases barrier height and thus suppresses leakage current.

The frequency-dependent C - V and G/ω - V characteristics of Pt/GaN and Pt/Gr/GaN SBDs measured at room temperature in the frequency range from 1 kHz to 1 MHz are shown in Fig. 5. In the reverse bias region, the lines dispersion is very small. While in forward bias, a drastic variation in frequency-dependent C - V and G/ω - V plots have been observed as shown in Fig. 5(a-d). The capacitance value increases with increasing forward bias, and an anomalous peak appears. The magnitude of the peak increases with decreasing frequency and show strong dispersion at lower frequency for both SBDs. The values of negative capacitance are found in forward bias at high frequencies. These phenomena could be attributed to the interface states [3,34-36]. According to the modified Schottky-Read model which imagines the presentation of impact-loss of electrons at the occupied interface states under injection of hot electrons [34], The change of the interface charge at different trap states produces anomalous behavior as well as negative capacitance. The differences in the anomalous behaviors between Pt/Gr/GaN

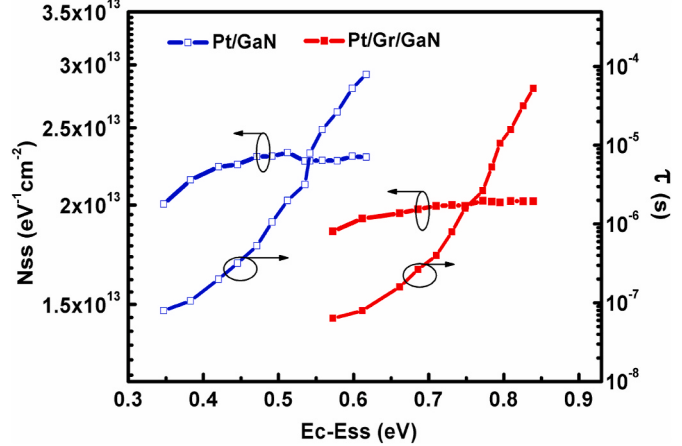


Fig. 7. The distribution and variation of the interface states density and time constant as a function of $E_c - E_{ss}$ for Pt/Gr/GaN and Pt/GaN SBDs at room temperature.

and Pt/GaN SBDs are distinct. As shown in Fig. 5(a-b), The magnitude of the corresponding peak for the Pt/Gr/GaN device is smaller than that of the Pt/GaN device. And the corresponding value of the forward applied voltage where the anomalous peak occurs for Pt/Gr/GaN SBD is higher than that of the Pt/GaN device. As shown in Fig. 5(c-d), the value of conductance increases rapidly with the increasing bias. In a given bias, the value of conductance increases with the decreasing of frequency, and the conductance of Pt/Gr/GaN SBDs is higher than that of Pt/GaN SBDs for each operating frequency.

The N_{ss} is extracted using the conductance method [37]. It should be noted that we assume the existence of a native oxide layer or graphene-native oxide layer between the metal and semiconductor. In order to estimate the interface states, the equivalent parallel conductance G_p is extracted from the following equation:

$$\frac{G_p}{\omega} = \frac{\omega C_i^2 G_m}{G_m^2 + \omega^2(C_i - C_m)^2} \quad (7)$$

where ω is the angular frequency of measurement, C_i is the capacitance of the interfacial layer which is extracted from current-voltage measurements [38,39]. G_m and C_m are measured conductance and capacitance respectively. The calculated G_p/ω using (7) versus measurement frequency for Pt/Gr/GaN and Pt/GaN SBDs are plotted in Fig. 6(a) and (b), respectively.

From the conductance peak, the interface state density is given by Refs. [35,40]:

$$N_{ss} \approx \frac{2.5}{qA} \left(\frac{G_p}{\omega} \right)_{peak} \quad (8)$$

The energy of interface states E_{ss} with respect to the bottom of the

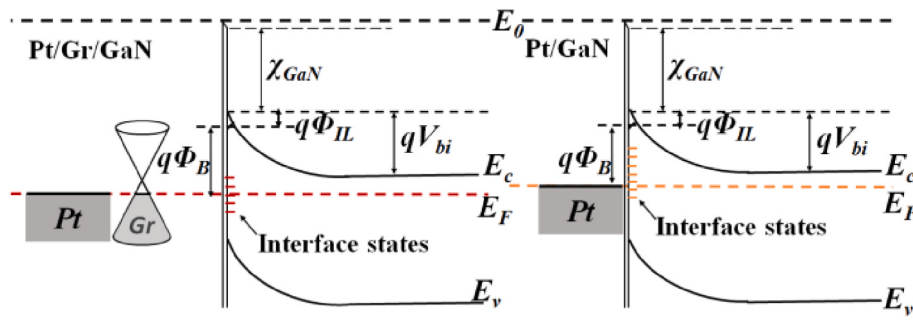


Fig. 8. Schematic band diagrams of Pt/Gr/GaN and Pt/GaN Schottky contact, in which a thin interfacial layer and interface states are considered.

conduction band at the surface of n-type semiconductor can be expressed as $E_c - E_{ss} = q(\Phi_B - V)$ [40,41]. Here the Φ_B is the barrier height extracted from the C-V measurement. The distribution and variation of N_{ss} and their time constant τ as a function of $(E_c - E_{ss})$ for the devices of Pt/GaN SBD and Pt/Gr/GaN at room temperature are shown in Fig. 7. The values of N_{ss} for the Pt/GaN SBD vary in the range of 2×10^{13} to $2.33 \times 10^{13} \text{ eV}^{-1}\text{cm}^{-2}$ at $(E_c - 0.35)$ to $(E_c - 0.62) \text{ eV}$, while those of Pt/Gr/GaN SBD vary in the range of 1.85×10^{13} to $2.02 \times 10^{13} \text{ eV}^{-1}\text{cm}^{-2}$ at $(E_c - 0.57)$ to $(E_c - 0.84) \text{ eV}$. It shows that the N_{ss} of with Gr Schottky interlayer is lower than that of without Gr interlayer. The N_{ss} distribution of Pt/Gr/GaN SBD shifts toward the mid-gap of the GaN compared to that of Pt/GaN SBD. The time constant τ was determined from the frequency corresponding to the G_p/ω peak. The τ exponentially increase with increasing $E_c - E_{ss}$ as shown in Fig. 7. It can be seen that the values of the τ for the two types of SBDs lie in a similar range from about $8 \times 10^{-8} \text{ s}$ to $6 \times 10^{-5} \text{ s}$ though corresponding to different energy levels. The time constants affect the frequency-dependent characteristics of the devices. This also explains that some frequency-dependent characteristics of the two type devices appear at a similar frequency.

The results suggest that the presence of Gr interlayer between metal and GaN has an obvious effect on interface states. As the chemically inert 2D material without dangling bonds, Gr suppresses the formation of interface states at Gr/semiconductor interface [42]. This can result in the reduction of the interface states for Pt/Gr/GaN SBDs. The property of the interface states is strongly related to the characteristic of the SBH, anomalous peaks observed in C-V-T and G/o-V-T measurements. It is considered that the reduction of the interface states leads to a reduced intensity of the capacitance anomalous peaks [34,36,43–45]. The band diagrams considering the interface states are schematically displayed in Fig. 8. According to the Bardeen model, the interface states lead to the Femi level pinning effect. The N_{ss} distribution is more toward the mid-gap of GaN for Pt/Gr/GaN SBD. This means the existence of deeper traps at the interface introduced by the Gr interlayer leads to the lower Femi level which increases Schottky barrier height in Pt/Gr/GaN compared to that of Pt/GaN SBD.

4. Conclusion

The modulated effects of Gr interlayer on the electrical properties of Pt/GaN SBDs are investigated. The results indicate that Pt/Gr/GaN SBD exhibits higher SBH and lower leakage current. The $\varphi_{B,CV}$ increases from 0.89 eV to 1.35 eV at room temperature by the introduction of Gr interlayer between Pt and GaN. The improved leakage characteristics of Pt/Gr/GaN are attribute to the Gr interlayer which increases barrier height and suppresses leakage. The N_{ss} with Gr interlayer is reduced from the range of 2×10^{13} – $2.33 \times 10^{13} \text{ eV}^{-1}\text{cm}^{-2}$ at $(E_c - 0.35)$ to $(E_c - 0.62) \text{ eV}$ to the range of 1.85×10^{13} – $2.02 \times 10^{13} \text{ eV}^{-1}\text{cm}^{-2}$ at $(E_c - 0.57)$ to $(E_c - 0.84) \text{ eV}$. The time constants τ for the two types of SBDs lie in a similar range from about $8 \times 10^{-8} \text{ s}$ to $6 \times 10^{-5} \text{ s}$. The modulated effects could be attributed to the Gr interlayer which is a chemically inert 2D material without dangling bonds and modulates the density and

distribution of interface states at metal/semiconductor interface.

CRediT authorship contribution statement

Junxue Ran: Conceptualization, Investigation, Writing – original draft. **Yijian Song:** Formal analysis, Investigation. **Xiaoli Ji:** Funding acquisition, Writing – review & editing. **Renfeng Chen:** Data curation, Methodology. **Jiankun Yang:** Formal analysis, Writing – review & editing. **Junxi Wang:** Funding acquisition, Resources, Supervision. **Tongbo Wei:** Formal analysis, Project administration, Supervision, Writing – review & editing.

Declaration of competing interest

The authors declare that they have no known competing financial interests or personal relationships that could have appeared to influence the work reported in this paper.

Data availability

Data will be made available on request.

Acknowledgments

The authors would like to thank Dr. Bingzhi Liu and Dr. Jingyu Sun at Beijing Graphene Institute for the graphene material preparation. This work was financially supported by Beijing Natural Science Foundation (Nos. 4222079 and 4222077), the National Key R&D Program of China (No. 2021YFB3602401), the National Natural Science Foundation of China (No. 52192614) and GuangDong Basic and Applied Basic Research Foundation (Grant 2022B1515120081).

References

- [1] H.C. Casey, G.G. Fountain, R.G. Alley, B.P. Keller, S.P. DenBaars, *Appl. Phys. Lett.* 68 (1996) 1850–1852.
- [2] S.O. Tan, İ. Taşçuoğlu, Ş. Altindal, *IEEE Trans. Electron. Dev.* 68 (2021) 5085–5089.
- [3] Ç.Ş. Güçlü, A.F. Özdemir, A. Karabulut, A. Kökce, Ş. Altindal, *Mater. Sci. Semicond. Process.* 89 (2019) 26–31.
- [4] M. Fagerlind, F. Allerstam, E.O. Sveinbjörnsson, N. Rorsman, A. Kakanakova-Georgieva, A. Lundskog, U. Forsberg, E. Janzen, *J. Appl. Phys.* 108 (2010) 014508.
- [5] X. Wang, Y. Zhang, S. Huang, H. Yin, J. Fan, K. Wei, Y. Zheng, W. Wang, H. Jiang, X. Wu, X. Wang, C. Liu, X. Liu, ACS Appl. Mater. Interfaces 13 (2021) 7725.
- [6] S. Huang, Q. Jiang, S. Yang, C. Zhou, K.J. Chen, *IEEE Electron. Device Lett.* 33 (2012) 516–518.
- [7] M. Ulusoy, Y. Badali, G. P-Givi, Y. Azizian-Kalandaragh, Ş. Altindal, *Synth. Met.* 292 (2023) 117243.
- [8] M. Ulusoy, Ş. Altindal, Y. Azizian-Kalandaragh, S. Özçelik, Z. Mirzaei-Kalar, *Microelectron. Eng.* 258 (2022) 111768.
- [9] H. Tecimer, S.O. Tan, Ş. Altindal, *IEEE Trans. Electron. Dev.* 65 (2018) 231–236.
- [10] K.S. Novoselov, A.K. Geim, S.V. Morozov, D.Y. JiangZhang, S.V. Dubonos, I. V. Grigorieva, A.A. Firsov, *Science* 306 (2004) 666–669.
- [11] Y.J. Lin, J.J. Zeng, *Phys. Lett.* 102 (2013) 183120.
- [12] A. Vitale, H. Murad, A. Abdelhafiz, P. Buntin, F.M. Alamgir, *ACS Appl. Mater. Interfaces* 11 (2018) 1026.
- [13] S. Sonde, F. Giannazzo, V. Raineri, R. Yakimova, J.R. Huntzinger, A. Tiberj, J. Camassel, *Phys. Rev. B* 80 (2009) 241406.

- [14] H.H. Yoon, S. Jung, G. Choi, J. Kim, Y. Jeon, Y.S. Kim, H.Y. Jeong, K. Kim, S. Y. Kwon, K. Park, *Nano Lett.* 17 (2017) 44–49.
- [15] X. Li, H. Zhu, *Phys. Today* 69 (2016) 46–51.
- [16] P. Zhang, Y. Zhang, Y. Wei, H. Jiang, X. Wang, Y. Gong, *J. Semiconduct.* 41 (2020) 071901.
- [17] F. Giannazzo, G. Greco, E. Schiliro, R.L. Nigro, I. Deretziis, A.L. Magna, F. Roccaforte, F. Iucolano, S. Ravesi, E. Frayssinet, A. Michon, Y. Cordier, *ACS Appl. Electron. Mater.* 1 (2019) 2342–2354.
- [18] P. Prystawko, F. Giannazzo, M. Krysko, J. Smalc-Koziorowska, E. Schiliro, G. Greco, F. Roccaforte, M. Leszczynski, *Mater. Sci. Semicond. Process.* 93 (2019) 153–157.
- [19] A. Zubair, A. Nourbakhsh, J.Y. Hong, M. Qi, Y. Song, D. Jena, J. Kong, M. Dresselhaus, T. Palacios, *Nano Lett.* 17 (2017) 3089–3096.
- [20] S. Tongay, M. Lemaitre, T. Schumann, K. Berke, B.R. Appleton, B. Gila, A. F. Hebard, *Appl. Phys. Lett.* 99 (2011) 102102.
- [21] G. Fisichella, G. Greco, F. Roccaforte, F. Giannazzo, *Nanoscale* 6 (2014) 8671–8680.
- [22] G. Kalita, M.D. Shaarin, B. Paudel, R. Mahyavanshi, M. Tanemura, *Appl. Phys. Lett.* 111 (2017) 013504.
- [23] M. Dub, P. Sai, A. Przewioka, A. Krajewska, M. Sakowicz, P. Prystawko, J. Kacerski, I. Pasternak, G. Cywinski, D. But, W. Knap, S. Rumyantsev, *Materials* 13 (2020) 4140.
- [24] J. Yu, M. Shafiei, J. Ou, K. Shin, W. Wlodarski, *IEEEExplore* (2012), <https://doi.org/10.1109/ICSENS.2011.6126969>.
- [25] S. Kim, T.H. Seo, M.J. Kim, K.M. Song, E.K. Suh, H. Kim, *Nano Res.* 8 (2015) 1327–1338.
- [26] J. Ran, B. Liu, X. Ji, A. Fariza, Z. Liu, J. Wang, P. Gao, T. Wei, *J. Phys. D Appl. Phys.* 53 (2020) 404003.
- [27] Z. Chen, Q. Yue, X. Chen, Y. Zhang, Z. Liu, *Adv. Mater.* 31 (2019) 1803639.
- [28] D. Korucu, S. Duman, A. Turut, *Mater. Sci. Semicond. Process.* 30 (2015) 393–399.
- [29] H. Fu, H. Chen, X. Huang, I. Baranowski, J. Montes, T. Yang, Y. Zhao, *IEEE Trans. Electron. Dev.* 65 (2018) 3507–3513.
- [30] T. Maeda, M. Okada, M. Ueno, Y. Yamamoto, T. Kimoto, Ma Horita, J. Suda, *Appl. Phys. Express* 10 (2017) 051002.
- [31] H. Teisseyre, P. Perlin, T. Suski, I. Grzegory, S. Porowski, J. Jun, *J. Appl. Phys.* 76 (1994) 2429–2434.
- [32] Kadir Ejderha, A. Turut, *J. Electron. Mater.* 50 (2021) 6741–6747.
- [33] T. Hatakeyama, T. Shinohne, *Mater. Sci. Forum* 1169 (2002) 389–393.
- [34] X. Wu, E.S. Yang, H.L. Evans, *J. Appl. Phys.* 68 (1990) 2845–2848.
- [35] Z. Berktaş, E. Orhan, M. Ulusoy, M. Yıldız, Ş. Altindal, *ACS Appl. Electron. Mater.* 5 (2023) 1804–1811.
- [36] M.H. Al-Dharob, A. Kökce, D.A. Aldemir, A.F. Özdemir, Ş. Altindal, *J. Phys. Chem. Solid.* 144 (2020) 109523.
- [37] E.H. Nicollian, A. Goetzberger, *Bell syst. Tech. J.* 46 (1967) 1055–1133.
- [38] J.M. Andrews, M.P. Lepsetler, *Solid State Electron.* 13 (1970) 1011–1023.
- [39] S. Wang, Y. Zhang, Y. Zhang, Chin, *Phys.* 12 (2003) 94–96.
- [40] S.K. Gupta, B. Shankar, W.R. Taube, J. Singh, J. Akhtar, *Physica B* 434 (2014) 44–50.
- [41] N. Shiwakoti, A. Bobby, B. Antony, K. Asokan, *J. Vac. Sci. Technol. B*, 34 (2016) 051206.
- [42] H. Yang, J. Heo, S. Park, H.J. Song, D.H. Seo, K. Byun, P. Kim, I. Yoo, H. Chung, K. Kim, *Science* 336 (2012) 1140–1142.
- [43] P.S. Ho, E.S. Yang, H.L. Evans, X. Wu, *Phys. Rev. Lett.* 56 (1986) 177–180.
- [44] P. chattopadhyay, B. Raychaudhuri, *Solid State Electron.* 36 (1993) 605–610.
- [45] B. Akin, Ş. Altindal, *Physica B* 594 (2020) 412274.